# Supplementary Data

## Appendix A – Supporting experimental data

The EDX elemental map shown in Fig. A1 confirms that the large second phase precipitates at the grain boundaries are rich in Al and Zr.

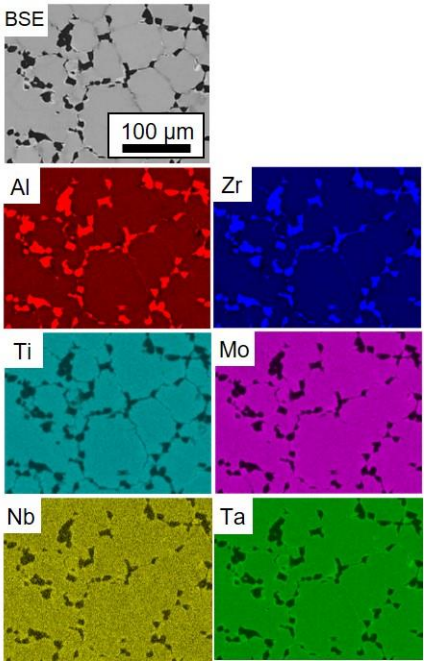


**Fig. A1.** EDX element Mapping of the AN alloy.

The EBSD pattern quality (PQ), inverse pole figure in Z (IPFZ) and phase map of the RSA in the AN are respectively shown in Fig. A2a-c. The EDX-coupled EBSD system indexes the large equiaxed grains in Fig. A2c as "BCC" with a composition rich in Nb, Ti and Zr. The IPFZ Map shows no sign of crystallographic texture of the large A2/B2 grains. The precipitates located at the grain boundaries are indexed as a hexagonal crystal structure with a composition rich in Al and Zr. The hexagonal intermetallic phase shows a trend of preferred orientation (mostly blue in Fig. A2b) along various grain boundaries and across grains.

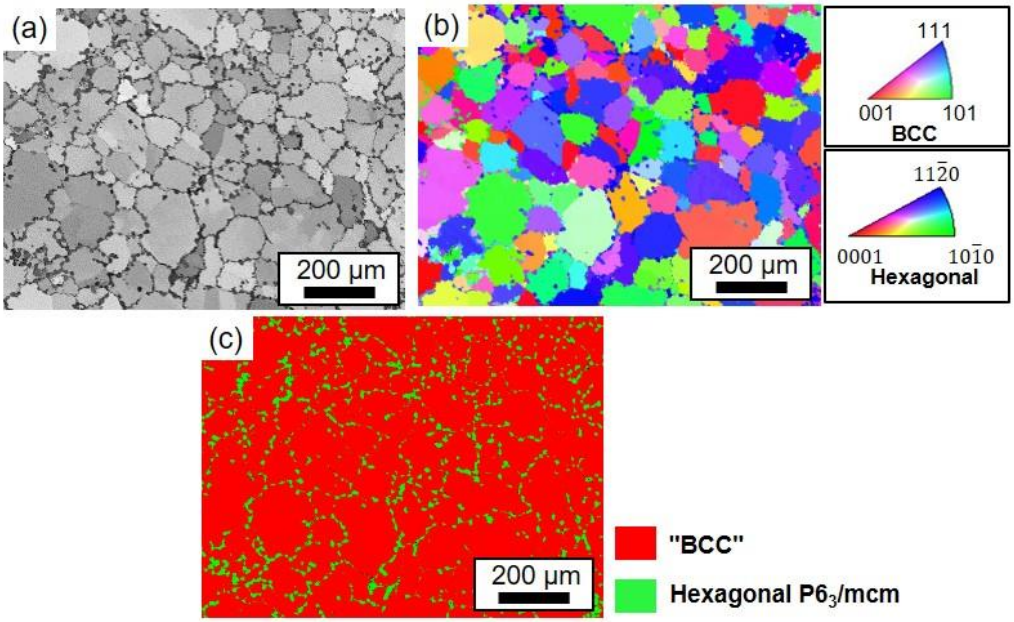

**Fig. A2.** EBSD maps of RSA in AN state. (a) pattern quality map, (b) inverse pole figure (IPFZ) map and (c) phase map identifying a BCC phase and the hexagonal $P6_3/mcm$.

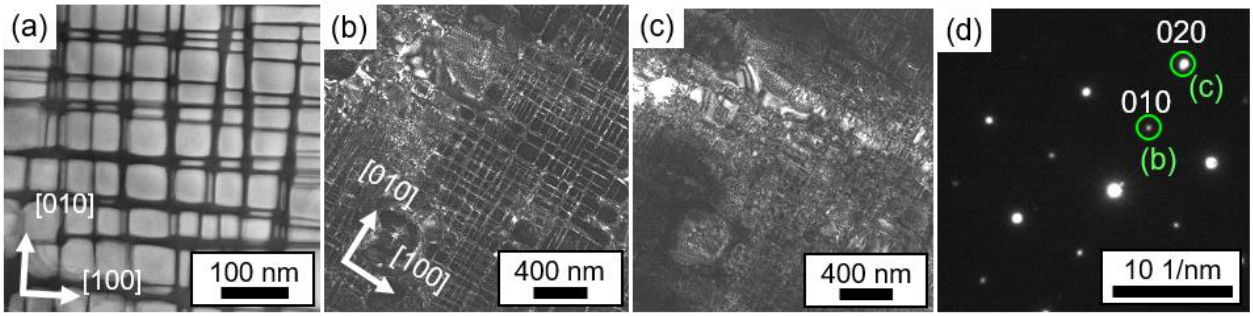


**Fig. A3.** (a) STEMDF micrograph of the RSA after annealing at 1400 °C for 24 hours oriented along [001] zone axis. (C)TEM-DF micrographs of the nanostructure in the equiaxed grains oriented along [010] zone axis. (b) DF3, using superlattice reflection 010 in (d). (c) DF4, using reflection 020. (d) SADP with contrast apertures marked in green for DF3 (b), DF4 (c).

A closer look into the center of a grain indexed as "BCC" via EBSD is presented by using TEM in Fig. A3 on a grain cut close to (001) and correspondingly imaged along the [001] zone axis. The enhanced atomic number contrast in the STEM-HAADF image of Fig. A3a, similar to the SEM-BSE micrograph in **Fehler! Verweisquelle konnte nicht gefunden werden.**d (main manuscript), reveals the nanostructure known to be characteristic for this alloy. The STEM-DF micrograph shows a heterogeneous nanostructure that consists of bright (larger mean atomic number, $\overline{Z}$) cuboidal (edge length < 100 nm) and plate-like (thickness ≈ 10 – 100 nm) precipitates embedded in a continuous darker (lower $\overline{Z}$) phase (thickness ≈ 3 – 30 nm). Fig. A3b-c show CTEM-DF images, respectively associated to the 010 and 020 reflections marked in green on their corresponding SADP (Fig. A3d). In green, Fig. A3d shows the location of the apertures, which leads to the diffraction contrasts in Fig. A3b-c. The microstructure reports a mixture of channels / precipitates with B2 (lower $\overline{Z}$) / A2 (higher $\overline{Z}$) phase, respectively.

## Appendix B – Supporting CALPHAD calculations

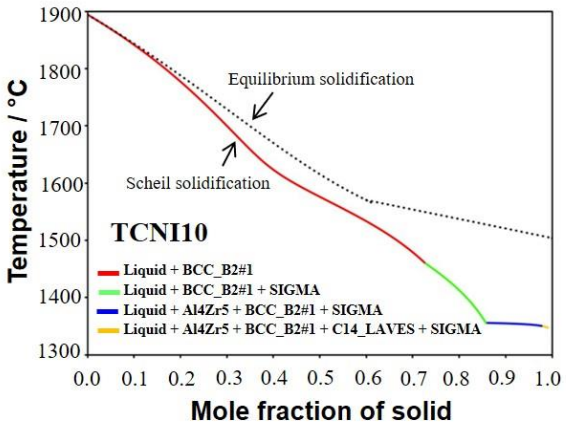


**Fig. B1.** Scheil solidification diagram for the RSA using the Thermo-Calc software with database TCNI10 database.

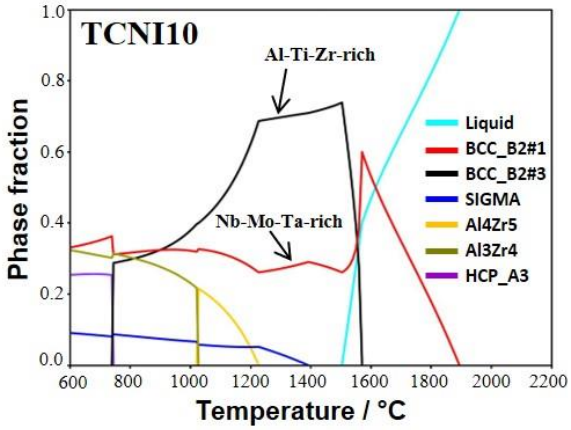


**Fig. B2.** Property diagram for the RSA using Thermo-Calc software (TCNI10 database).

**Table B1.** Equilibrium phase transformation temperatures (in °C) in the studied alloys. Simulated results using TCHEA3 database.

| Phase Transformation | T (°C) |
|---|---|
| L → BCC_B2#1 + L | 1895 |
| L → BCC_B2#1 + BCC_B2#3 + L | 1570 |
| L → BCC_B2#1 + BCC_B2#3 | 1505 |
| BCC_B2#1 + BCC_B2#3 → BCC_B2#1 + BCC_B2#3 + SIGMA | 1388 |
| BCC_B2#1 + BCC_B2#3 + SIGMA → BCC_B2#1 + BCC_B2#3 + SIGMA + Al4Zr5 | 1225 |
| BCC_B2#1 + BCC_B2#3 + SIGMA + Al4Zr5 → BCC_B2#1 + BCC_B2#3 + SIGMA + Al3Zr4 | 1025 |
| BCC_B2#1 + BCC_B2#3 + SIGMA + Al3Zr4 → BCC_B2#1 + SIGMA + Al3Zr4 + HCP_A3 | 743 |

**Table B2.** Equilibrium phase transformation temperatures (in °C) in the studied alloys. Simulated results using TCNI10 database.

| Phase Transformation | T (°C) |
|---|---|
| L → BCC_B2#1 + L | 1895 |
| L → BCC_B2#1 + BCC_B2#3 + L | 1570 |
| L → BCC_B2#1 + BCC_B2#3 | 1505 |
| BCC_B2#1 + BCC_B2#3 → BCC_B2#1 + BCC_B2#3 + SIGMA | 1388 |
| BCC_B2#1 + BCC_B2#3 + SIGMA → BCC_B2#1 + BCC_B2#3 + SIGMA + Al4Zr5 | 1225 |
| BCC_B2#1 + BCC_B2#3 + SIGMA + Al4Zr5 → BCC_B2#1 + BCC_B2#3 + SIGMA + Al3Zr4 | 1025 |
| BCC_B2#1 + BCC_B2#3 + SIGMA + Al3Zr4 → BCC_B2#1 + SIGMA + Al3Zr4 + HCP_A3 | 743 |

**Table B3.** Calculated elements mole fractions of equilibrium phases in the studied alloy at T = 1000 °C (1273 K). Database TCHEA3.

| Phases | Sublattice | Al | Ti | Zr | Nb | Mo | Ta | Phase rich in |
|---|---|---|---|---|---|---|---|---|
| BCC_B2_#1 | 1 | 0.04 | 0.16 | 0.02 | 0.44 | 0.24 | 0.10 | Mo-Nb-Ta |
| | 2 | 0.04 | 0.16 | 0.02 | 0.44 | 0.24 | 0.10 | |
| BCC_B2_#3 | 1 | 0.20 | 0.41 | 0.20 | 0.14 | 0.04 | 0.01 | Al-Ti-Zr |
| | 2 | 0.20 | 0.41 | 0.20 | 0.14 | 0.04 | 0.01 | |
| Al3Zr4 | 1 | 1.00 | 0.00 | 0.00 | 0.00 | 0.00 | 0.00 | Al-Zr |
| | 2 | 0.00 | 0.00 | 1.00 | 0.00 | 0.00 | 0.00 | |
| SIGMA | 1 | 0.98 | 0.00 | 0.00 | 0.01 | 0.00 | 0.01 | - |
| | 2 | 0.00 | 0.00 | 0.00 | 0.01 | 0.98 | 0.01 | |
| | 3 | 0.00 | 0.00 | 0.00 | 0.17 | 0.00 | 0.83 | |

**Table B4.** Calculated elements mole fractions of equilibrium phases in the studied alloy at T = 1000 °C (1273 K). Database TCNI10.

| Phases | Sublattice | Al | Ti | Zr | Nb | Mo | Ta | Phase rich in |
|---|---|---|---|---|---|---|---|---|
| BCC_B2_#1 | 1 | 0.04 | 0.16 | 0.02 | 0.44 | 0.24 | 0.10 | Mo-Nb-Ta |
| | 2 | 0.04 | 0.16 | 0.02 | 0.44 | 0.24 | 0.10 | |
| BCC_B2_#3 | 1 | 0.20 | 0.41 | 0.20 | 0.14 | 0.04 | 0.01 | Al-Ti-Zr |
| | 2 | 0.20 | 0.41 | 0.20 | 0.14 | 0.04 | 0.01 | |
| Al3Zr4 | 1 | 1.00 | 0.00 | 0.00 | 0.00 | 0.00 | 0.00 | Al-Zr |
| | 2 | 0.00 | 0.00 | 1.00 | 0.00 | 0.00 | 0.00 | |
| SIGMA | 1 | 0.98 | 0.00 | 0.00 | 0.01 | 0.00 | 0.01 | - |
| | 2 | 0.00 | 0.00 | 0.00 | 0.01 | 0.98 | 0.01 | |
| | 3 | 0.00 | 0.00 | 0.00 | 0.17 | 0.00 | 0.83 | |

**Table B5.** Calculated elements mole fractions of equilibrium phases in the studied alloy at T = 1500 °C (1773 K). Database TCNI10

| **Phases** | Sublattice | **Al** | **Ti** | **Zr** | **Nb** | **Mo** | **Ta** | **Phase rich in** |
|---|---|---|---|---|---|---|---|---|
| **BCC_B2_#3** | 1 | 0.25 | 0.22 | 0.27 | 0.16 | 0.06 | 0.04 | Al-Ti-Zr |
| | 2 | 0.25 | 0.22 | 0.27 | 0.16 | 0.06 | 0.04 | |
| **BCC_B2_#1** | 1 | 0.09 | 0.17 | 0.06 | 0.32 | 0.21 | 0.15 | Mo-Nb-Ta |
| | 2 | 0.09 | 0.17 | 0.06 | 0.32 | 0.21 | 0.15 | |

**Table B6.** Calculated elements mole fractions of equilibrium phases in the studied alloy at T = 1500 °C (1773 K). Database TCHEA3

| **Phases** | Sublattice | **Al** | **Ti** | **Zr** | **Nb** | **Mo** | **Ta** | **Phase rich in** |
|---|---|---|---|---|---|---|---|---|
| **BCC_B2_#3** | 1 | 0.25 | 0.22 | 0.27 | 0.16 | 0.06 | 0.04 | Al-Ti-Zr |
| | 2 | 0.25 | 0.22 | 0.27 | 0.16 | 0.06 | 0.04 | |
| **BCC_B2_#1** | 1 | 0.09 | 0.17 | 0.06 | 0.32 | 0.21 | 0.15 | Mo-Nb-Ta |
| | 2 | 0.09 | 0.17 | 0.06 | 0.32 | 0.21 | 0.15 | |

**Table B7.** Calculated elements mole fractions of equilibrium phases in the studied alloy at T = 700 °C (973 K). Database TCNI10

| **Phases** | Sublattice | **Al** | **Ti** | **Zr** | **Nb** | **Mo** | **Ta** | **Phase rich in** |
|---|---|---|---|---|---|---|---|---|
| **BCC_B2#1** | 1 | 0.01 | 0.10 | 0.00 | 0.55 | 0.26 | 0.08 | Nb-Mo-Ta |
| | 2 | 0.01 | 0.10 | 0.00 | 0.55 | 0.26 | 0.08 | |
| **Al3Zr4** | 1 | 1.00 | 0.00 | 0.00 | 0.00 | 0.00 | 0.00 | Al-Zr |
| | 2 | 0.00 | 0.00 | 1.00 | 0.00 | 0.00 | 0.00 | |
| **HCP_A3** | 1 | 0.18 | 0.66 | 0.13 | 0.03 | 0.00 | 0.00 | Al-Ti-Zr |
| | 2 | VA | VA | VA | VA | VA | VA | |
| **SIGMA** | 1 | 1.00 | 0.00 | 0.00 | 0.00 | 0.00 | 0.00 | - |
| | 2 | 0.00 | 0.00 | 0.00 | 0.01 | 0.99 | 0.00 | |
| | 3 | 0.00 | 0.00 | 0.00 | 0.08 | 0.00 | 0.92 | |

**Table B8.** Calculated elements mole fractions of equilibrium phases in the studied alloy at T = 700 °C (973 K). Database TCHEA3

| **Phases** | Sublattice | **Al** | **Ti** | **Zr** | **Nb** | **Mo** | **Ta** | **Phase rich in** |
|---|---|---|---|---|---|---|---|---|
| **BCC_B2#1** | 1 | 0.01 | 0.10 | 0.00 | 0.55 | 0.26 | 0.08 | Nb-Mo-Ta |
| | 2 | 0.01 | 0.10 | 0.00 | 0.55 | 0.26 | 0.08 | |
| **Al3Zr4** | 1 | 1.00 | 0.00 | 0.00 | 0.00 | 0.00 | 0.00 | Al-Zr |
| | 2 | 0.00 | 0.00 | 1.00 | 0.00 | 0.00 | 0.00 | |
| **HCP_A3** | 1 | 0.18 | 0.66 | 0.13 | 0.03 | 0.00 | 0.00 | Al-Ti-Zr |
| | 2 | VA | VA | VA | VA | VA | VA | |
| **SIGMA** | 1 | 1.00 | 0.00 | 0.00 | 0.00 | 0.00 | 0.00 | - |
| | 2 | 0.00 | 0.00 | 0.00 | 0.01 | 0.99 | 0.00 | |
| | 3 | 0.00 | 0.00 | 0.00 | 0.08 | 0.00 | 0.92 | |

**Table B9.** Calculated elements mole fractions of equilibrium phases in the studied alloy at 2000, 1700, 1520 and 1200 °C. Data base TCHEA3.

| Temperature (°C) | Phases | Volume fraction of phase | Sublattice | **Al** | **Ti** | **Zr** | **Nb** | **Mo** | **Ta** |
|---|---|---|---|---|---|---|---|---|---|
| 2000 | **Liquid** | 1.00 | | 0.21 | 0.21 | 0.21 | 0.20 | 0.10 | 0.07 |
| 1700 | **BCC_B2#1** | 0.32 | 1 | 0.10 | 0.21 | 0.07 | **0.33** | **0.18** | **0.11** |
| | | | 2 | 0.10 | 0.21 | 0.07 | **0.33** | **0.18** | **0.11** |
| | **Liquid** | 0.68 | | 0.27 | 0.21 | 0.28 | 0.13 | 0.06 | 0.05 |
| 1520 | **BCC_B2#1** | 0.26 | 1 | 0.10 | 0.18 | 0.07 | **0.32** | **0.20** | **0.13** |
| | | | 2 | 0.10 | 0.18 | 0.07 | **0.32** | **0.20** | **0.13** |
| | **BCC_B2#3** | 0.64 | 1 | **0.24** | **0.23** | **0.25** | 0.17 | 0.07 | 0.04 |
| | | | 2 | **0.24** | **0.23** | **0.25** | 0.17 | 0.07 | 0.04 |
| | **Liquid** | 0.10 | | 0.32 | 0.15 | 0.37 | 0.08 | 0.04 | 0.04 |
| 1200 | **BCC_B2#1** | 0.30 | 1 | 0.05 | 0.12 | 0.02 | **0.38** | **0.25** | **0.18** |
| | | | 2 | 0.05 | 0.12 | 0.02 | **0.38** | **0.25** | **0.18** |
| | **BCC_B2#3** | 0.70 | 1 | **0.28** | **0.25** | **0.30** | 0.12 | 0.03 | 0.02 |
| | | | 2 | **0.28** | **0.25** | **0.30** | 0.12 | 0.03 | 0.02 |

## Appendix C – Model crystal lattices

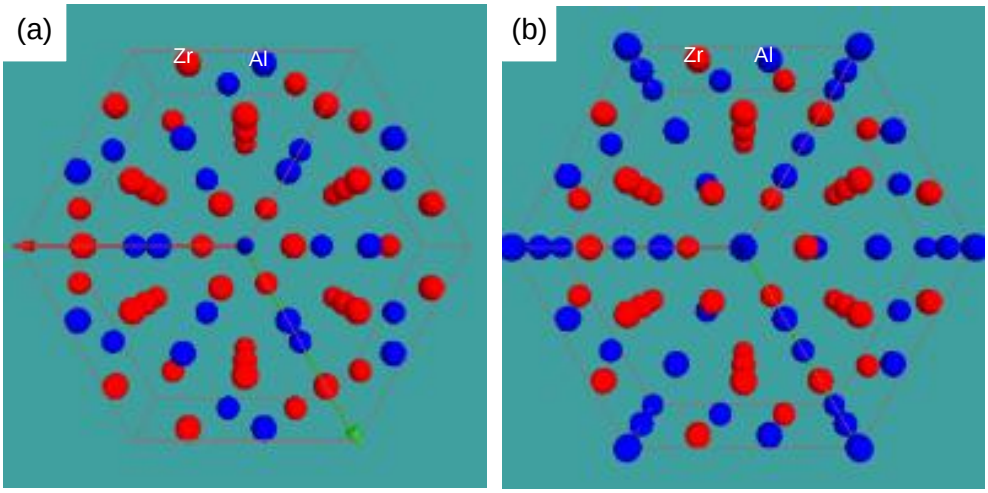


**Fig. C1.** Schematic representation of the crystalline structure of hexagonal Al-Zr phase (unit-cell) with (a) $Al_3Zr_5$ and (b) $Al_4Zr_5$ stoichiometry. Al atoms are in blue and Zr atoms are in red.